*Materials and Structures*, 1993, **26**, 30–37

# Effect of cold drawing on susceptibility to hydrogen embrittlement of prestressing steel

J. TORIBIO

*Department of Engineering, University of La Coruña*
*E.T.S.I. Caminos, Pol. Sabón, P.12–14, 15141 Arteixo, La Coruña, Spain*

A. M. LANCHA

*CIEMAT, Ciudad Universitaria, 28040 Madrid, Spain*

*This paper compares the behaviour under aggressive environmental conditions of a prestressing steel in two forms (bar and wire) of different yield strengths, to investigate the influence of this material parameter on their susceptibility to hydrogen-assisted cracking in aqueous environments. Slow strain-rate tests using pre-cracked specimens were performed under various environment conditions. Different fatigue pre-cracking loads were used to analyse the influence of the stress state in the vicinity of the crack tip on the hydrogen-assisted cracking process. The results confirm the well-known fact that the highest-strength steel is the most susceptible to hydrogen embrittlement. A model of hydrogen diffusion in metals – including the effects of both hydrogen concentration and hydrostatic stress distribution – is proposed to explain these results on the basis of the stress–strain curve of the material. Consideration is given to compressive residual stresses induced in the vicinity of the crack tip during the fatigue pre-cracking process. The model is able to explain the different susceptibility to hydrogen embrittlement of the two steels.*

## 1. INTRODUCTION

Two types of steel are commonly used in prestressed concrete: cold-drawn (C–Mn) or quenched and tempered (Si–Cr) steels. Both are high-strength steels, i.e., their yield strength is high enough to guarantee normal service in the elastic range. However, from the fracture mechanics point of view, they have less fracture toughness than ductile steels of lower yield strength. As a consequence, high-strength steels are more susceptible to surface defects or flaws such as cracks or notches [1].

Furthermore, prestressing steel wires usually work in aggressive environments, and can suffer stress corrosion cracking [2]. As a mechanism of environmentally assisted cracking (EAC), hydrogen embrittlement is a specific phenomenon which can be associated with all electrochemical conditions, not only under cathodic potentials but even under anodic ones [3].

The importance of hydrogen embrittlement led the International Prestressing Federation (FIP) to establish the well-known ammonium thiocyanate test [4] to determine the susceptibility of prestressing steels to such a phenomenon. This is a simple low-cost test but the scatter of the results is high [5,6]. Such scatter has been attributed to surface residual stress in the wires [7]. Recently, a model has been proposed to explain this on the basis of hydrogen diffusion in the steel [8].

The present work compares experimental results on hydrogen embrittlement of a prestressing steel in two forms (bar and wire) of different yield strengths. Consideration is given to the very important role of compressive residual stresses in the vicinity of crack tips after fatigue pre-cracking, which delay the entry of hydrogen and therefore the embrittlement process. To achieve this, very different fatigue pre-cracking loads were used, thereby providing distinct residual stress distributions in the aforementioned area. Finally, a non-conventional hydrogen diffusion model is proposed to explain the higher susceptibility of the cold-drawn wire to hydrogen embrittlement, by analysing the influence of the stress state in the vicinity of the crack tip on the hydrogen ingress into the sample.

## 2. EXPERIMENTAL PROCEDURE

The experimental programme included fracture tests in aggressive environments under various different electrochemical conditions (a large series of values for pH and potential). Tests were carried out at a constant extension rate with pre-cracked specimens. This procedure has advantages over other standard procedures: the scatter is lower and the environmental attack is located in the vicinity of the crack tip.

A high-strength eutectoid steel was used in this work. The chemical composition is given in Table 1. This steel was tested in two conditions: firstly, as hot-rolled patented cylindrical bars of 12 mm diameter and, secondly, as a commercial 7 mm diameter cold-drawn prestressing wire obtained from the bar.

After rolling, the 12-mm diameter bar was patented by

Table 1 Chemical composition of the steel (wt %)

| C | Mn | Si | P | S | Fe |
|---|---|---|---|---|---|
| 0.74 | 0.70 | 0.20 | 0.016 | 0.023 | balance |

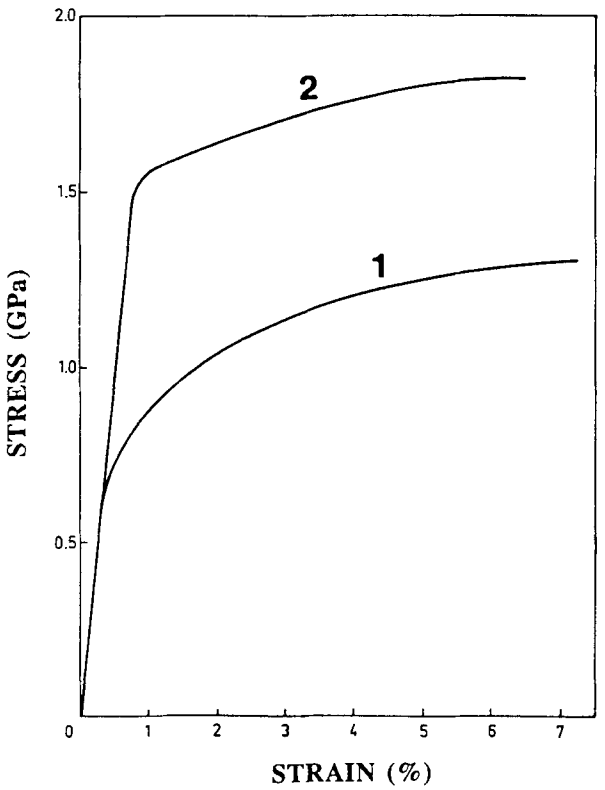


Fig. 1 Stress–strain curves of both steels: (1) hot-rolled, (2) cold-drawn.

cooling from the austenitic condition in a molten lead bath to produce fine pearlite. The wire was obtained by cold-drawing this bar in six passes, to achieve an overall reduction of 66%, and finally a stress-relieving process was applied involving exposure to about 400 °C for a few seconds. The mechanical properties of both the bar and the wire are presented in Table 2, and Fig. 1 shows the stress–strain curves for these materials. The fracture toughness $K_{IC}$ was determined using cylindrical pre-cracked specimens obtained from the bar and the wire – for which the plane strain condition is achieved at the inner points of the crack [1,9,10] – together with an expression for the maximum stress intensity factor at the

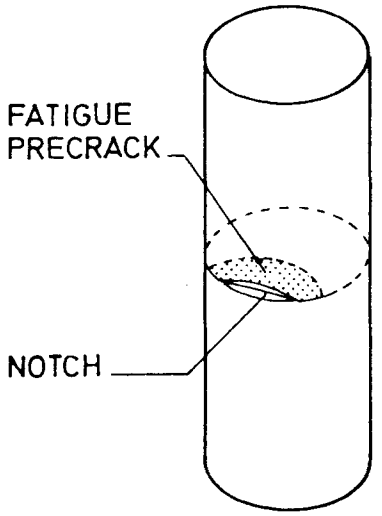


Fig. 2 Specimen geometry.

deepest point of the crack (assumed semi-elliptical) calculated by Astiz [11] using the finite element method (FEM) combined with a virtual crack extension technique.

The specimens used in the tests in an aggressive environment were transversely pre-cracked rods (Fig. 2). The transverse pre-crack was produced by axial fatigue, as described below. The relationship between crack depth and cylinder diameter was the same for all specimens: $a/D = 0.3$, i.e., $a = 4.0$ mm for the 12 mm diameter bars (hot-rolled), $a = 2.2$ mm for the 7 mm diameter wire (cold-drawn). Samples were coated with an insulating lacquer except for a band about 1 mm wide on each side of the notch and pre-crack.

Samples were subjected to slow strain-rate testing [12,13], a technique which has shown advantages over others [14]. The applied displacement rate was $8.3 \times 10^{-8}$ m s$^{-1}$, based on previous experience [3]. A fractographic analysis was carried out on the fractured samples [15], and the effects of the environmental conditions on fracture were quantified through the ratio of the failure load in the solution to the failure load in air.

Testing was performed at room temperature (between 16 and 22 °C). The aggressive environment was an aqueous solution of 1 g l$^{-1}$ $Ca(OH)_2$ plus 0.1 g l$^{-1}$ NaCl to which HCl was added in varying amounts to adjust the pH value below the value of 12.5 for the base solution (pH = 12.5, 8 and 4 were chosen). It has been suggested previously [3] that distilled water in contact with

Table 2 Mechanical properties of the bar and the wire

| Steel | Young's modulus (GPa) | Yield strength (MPa) | UTS (MPa) | Elongation under UTS (%) | Reduction of area (%) | Fracture toughness (MPa m$^{1/2}$) |
|---|---|---|---|---|---|---|
| Hot-rolled bar | 195 | 725 | 1300 | 8.0 | 30 | 53 |
| Cold-drawn wire | 190 | 1500 | 1830 | 5.8 | 37 | 84 |

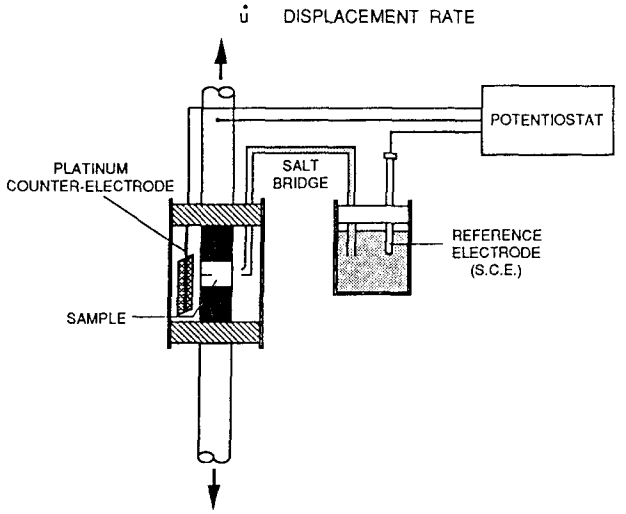


Fig. 3 Experimental device.

concrete usually achieved pH values in the vicinity of 12.5, being essentially a saturated solution of $Ca(OH)_2$, although other substances are likely to be present in small amounts, and the chloride ions may be expected to be present in many applications of concrete structures.

All tests were carried out at a constant potential covering a broad range from value $E = -100$ mV SCE (anodic) to the value $E = -1200$ mV SCE (cathodic). The experimental device is shown in Fig. 3, and consists of a potentiostat and a classical three-electrode assembly: metallic sample (working electrode), standard calomel electrode (reference electrode) and platinum wire (counterelectrode).

Pre-cracking of the samples was carried out in air. To evaluate the influence of the pre-cracking procedure, several types of sample were prepared by using different fatigue pre-cracking loads during the last step (just previous to the fracture test). Fig. 4 shows the fatigue programmes used to induce different degrees of compressive residual stress at the crack tip. The maximum fatigue pre-cracking loads used during the last step were 0.28 $K_{IC}$, 0.45 $K_{IC}$, 0.60 $K_{IC}$ and 0.80 $K_{IC}$.

## 3. RESULTS

Test variables were the pH of the solution, the electrochemical potential and the maximum fatigue load during pre-cracking. Results are presented in the very common form of the ratio of the failure load in solution to the failure load in air. The latter was obtained by performing two fracture tests in an air environment for each material [15].

A common characteristic for both materials at each of the three pH values is the existence of two regions of potential in which the effect of the environment reduces the failure loads. It appears that marked sensitivities to environmentally assisted cracking (EAC) become noticeable at potentials below about $-600$ mV SCE for pH 4, $-800$ mV SCE for pH 8 and $-900$ mV SCE for pH 12.5. A further regime of enhanced cracking appears

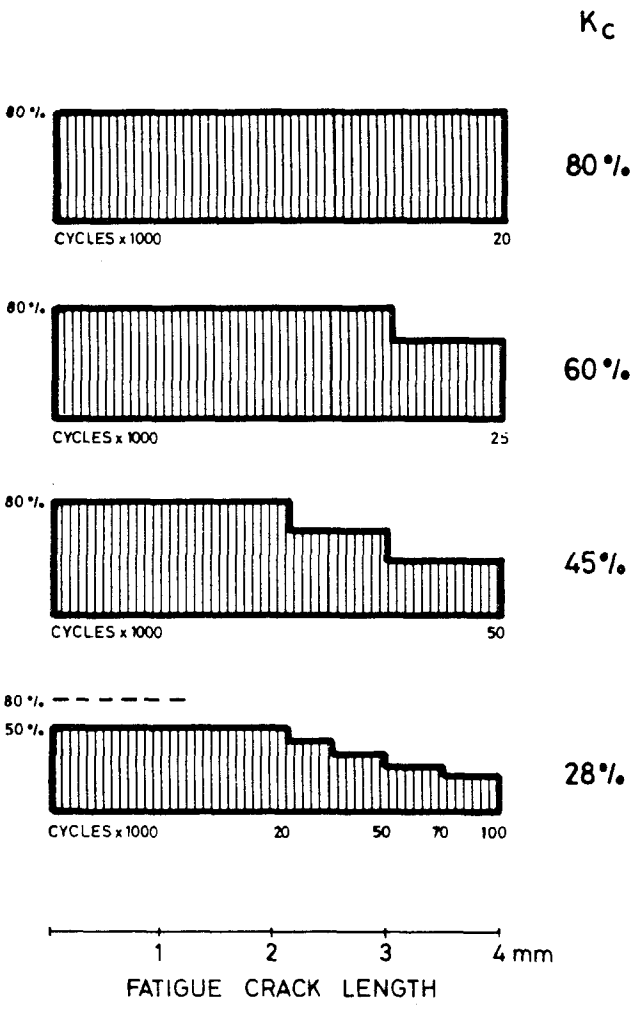


Fig. 4 Fatigue programmes used to induce different degrees of compressive residual stress at the crack tip.

at higher potentials. The region of higher potentials is the *anodic regime*, and the associated EAC mechanism is anodic dissolution; the region of lower potentials is the *cathodic regime*, and the associated mechanism is hydrogen embrittlement. There are, however, some uncertainties about the real electrochemical values at the crack tip, since the local environment within a crack differs from the bulk environment. Local acidification and therefore hydrogen embrittlement could be expected even at anodic potentials [16–20].

For a typical anodic regime ($-400$ mV) the results depend on pH (Fig. 5: hot-rolled bar, Fig. 6: cold-drawn wire). For the hot-rolled bar, the test severity decreases as the maximum fatigue load increases; in addition, the aggressiveness of the environment rises as the pH of the solution becomes more acid. The first effect is due to the compressive residual stresses in the vicinity of the crack tip, and the second, probably, to the coexistence of a mechanism of hydrogen embrittlement together with the anodic dissolution typical of these potentials, and to the higher chloride content which changes the electrochemical breakdown potential. For the cold-drawn wire, the test severity is almost independent of maximum fatigue load,

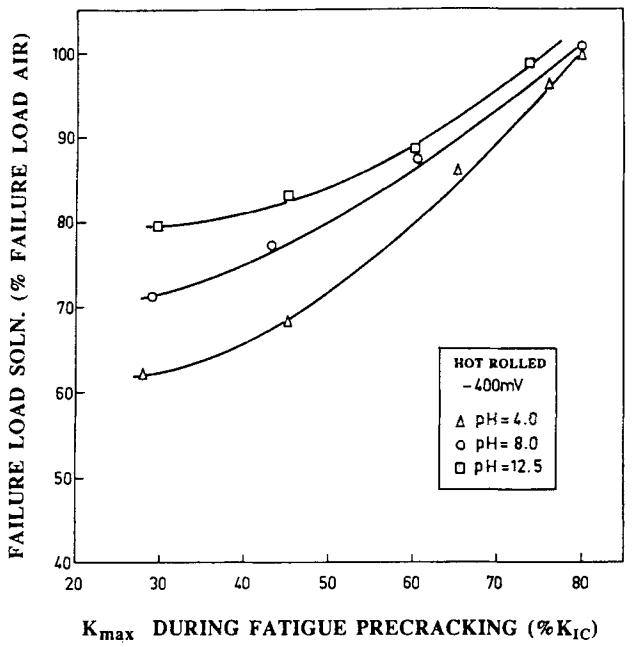


Fig. 5 Influence of fatigue load (hot-rolled, anodic regime).

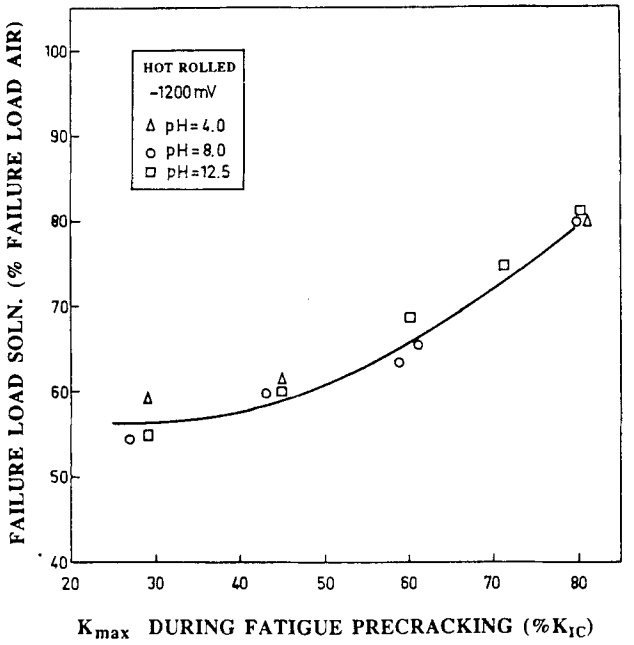


Fig. 7 Influence of fatigue load (hot-rolled, cathodic regime).

although it increases slightly as the pH becomes more acid. The explanation can be found in the fact that failure loads in solution and in air are really close, so that the effect of maximum fatigue load is negligible, although a slight pH effect can be observed due to the presence of either hydrogen or $Cl^-$ ions. The fundamental conclusion is that the cold-drawing process is beneficial from the EAC point of view at anodic potentials (anodic dissolution).

For a typical cathodic regime (−1200 mV) the results are practically independent of pH (Fig. 7: hot-rolled bar, Fig. 8: cold-drawn wire). For the hot-rolled bar, the test severity decreases as the maximum fatigue load increases, and this occurs for all values of $K_{max}$. For the cold-drawn wire, the effect is the same from the qualitative point of view (tendency), but not from the quantitative point of view (numerical values), because for all variability ranges of $K_{max}$ the behaviour of the cold-drawn steel is clearly below that of the hot-rolled one. Moreover, there are certain $K_{max}$ values ($K_{max} < 0.50\ K_{IC}$) for which the effect of the maximum fatigue load on the susceptibility of the cold-drawn wire to hydrogen embrittlement is negligible. The conclusion is that the cold-drawing process is damaging from the EAC point of view at cathodic

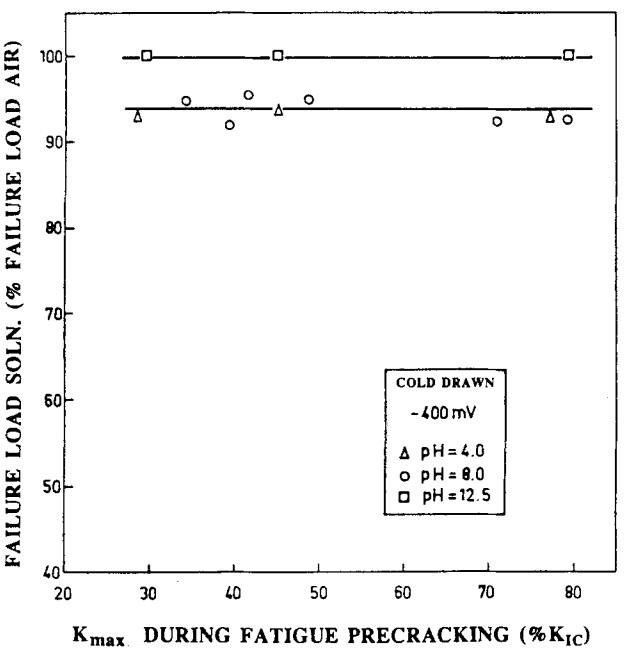


Fig. 6 Influence of fatigue load (cold-drawn, anodic regime).

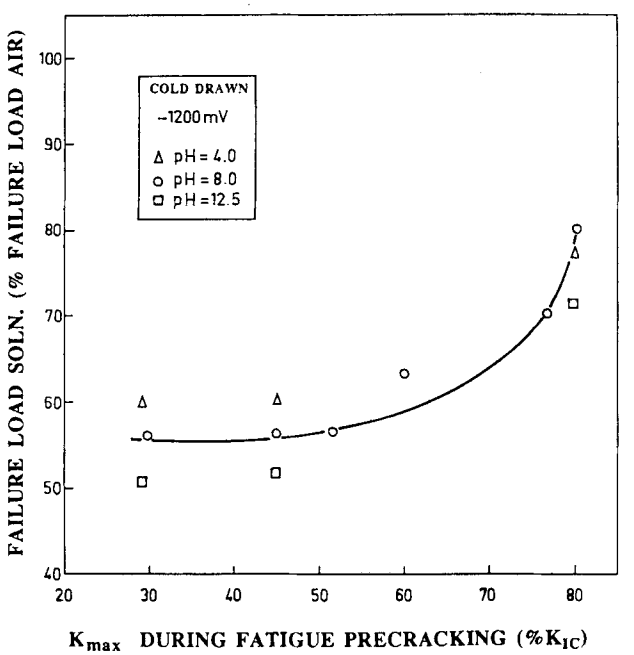


Fig. 8 Influence of fatigue load (cold-drawn, cathodic regime).

potentials (hydrogen embrittlement). This fact confirms previous results – not yet fully understood – with high-strength steels [21,22]. Therefore, the advantage of high strength – and the consequently increased bearing capacity in an air environment – is offset by the disadvantage of high susceptibility to hydrogen embrittlement.

The following section is devoted to discussing a plausible explanation of such a difference in behaviour of the two steels in the hydrogen environment used, with consideration of the important role of the residual stress distribution in the vicinity of the crack tip, which is modelled in a simple way and influences the hydrogen penetration into the sample in both situations.

## 4. DISCUSSION

The diffusion model includes not only transport of hydrogen towards the points of minimum concentration, but also towards those regions of maximum triaxial stress state. It is based on the three following assumptions:

1. The main transport mechanism of hydrogen in the metal is diffusion. This hypothesis is valid for high-strength pearlitic steels under environmental conditions of cathodic polarization as was demonstrated by Toribio and Elices [23]; the diffusion coefficient can depend, however, on temperature [24], concentration of hydrogen traps [25], sulphur content [26] or hydrogen pressure [27].
2. The absorption of hydrogen at the surface is quasi-instantaneous, as demonstrated in previous work [23]. As a consequence, the boundary condition for the diffusion problem is reached immediately.
3. Hydrogen does not modify the constitutive equation of the material, and therefore does not change the stress state in the metal. This hypothesis is valid for low hydrogen pressures, as in the case of hydrogen produced by electrochemical conditions.

The use of an effective hydrogen diffusion coefficient assumes that no differences in macroscopic behaviour could be expected due to hydrogen trapping in the two steels. Typical traps in high-strength steels are MnS inclusions [28], which do not introduce differences between two steels with the same chemical composition. Concerning dislocations, their effect is controversial and they produce two competing mechanisms, since they enhance the transport of hydrogen while increasing the amount of hydrogen traps.

Diffusion equations have been developed by Van Leeuwen [29] and Astiz [30], and these include not only the hydrogen concentration, but also the hydrostatic stress distribution. The flux density of hydrogen depends on the concentration and the hydrostatic stress gradients:

$$J = -D^* \operatorname{grad} c + Mc \operatorname{grad} \sigma \tag{1}$$

$$\frac{\partial c}{\partial t} = D^* \Delta c - M \operatorname{grad} c \cdot \operatorname{grad} \sigma - Mc\Delta\sigma \tag{2}$$

where $c$ is the hydrogen concentration, $t$ the time, $J$ the flux density vector, $\sigma$ the hydrostatic stress, $D^*$ the diffusion coefficient and $M$ a second coefficient, a function of the first:

$$M = \frac{D^* V^*}{RT} \tag{3}$$

in which $V^*$ is the partial molar volume of hydrogen, $R$ the ideal gas constant and $T$ the absolute temperature. The stationary solution is

$$c = c_0 \exp\left(\frac{V^* \sigma}{RT}\right) \tag{4}$$

i.e. a Boltzmann distribution where $c$ is the equilibrium concentration of hydrogen when the stress is zero, a constant which can be obtained from thermodynamic considerations [31]. In the stationary case the hydrogen concentration is a function only of the hydrostatic stress.

The geometry of the system is three-dimensional, since it is an edge crack in a cylinder. However, taking into account the plane strain assumption in the vicinity of the crack tip [1,9,10], it seems to be adequate to solve the problem in the plane of symmetry perpendicular to the crack at its deepest point (two-dimensional geometry). In this case, the hydrogen concentration at the sample boundary is not constant, but depends on the hydrostatic stress at the boundary points. Considering hypothesis 2, the hydrogen concentration at the boundary, $c_\Gamma$, has Boltzmann-type distribution:

$$c_\Gamma = c_0 \exp\left(\frac{V^* \sigma_\Gamma}{RT}\right) \tag{5}$$

where $\sigma_\Gamma$ represents the hydrostatic stress along the crack lips, varying as the distance from the crack tip increases. The hydrogen concentration at the crack tip is relevant, since there is a stress magnification at the point, which provides a path for the hydrogen ingress:

$$c_{CT} = c_0 \exp\left(\frac{V^* \sigma_{CT}}{RT}\right) \tag{6}$$

where $\sigma_{CT}$ represents the hydrostatic stress at the crack tip.

The hydrogen diffusion model proposed here allows a first explanation, at least qualitatively, of the experimental results for hydrogen embrittlement in both steels, summarized in Figs 7 and 8. Equations 1 and 2 show the importance, from the hydrogen diffusion point of view, of the hydrostatic stress in the vicinity of the crack tip: hydrogen flows not only towards the places with minimum concentration, but also towards those with maximum tensile hydrostatic stress. As a consequence, compressive residual stresses (created by plasticity in the vicinity of the crack tip during fatigue pre-cracking) reduce hydrogen entry and therefore delay the embrittlement.

Taking into account the stress–strain curves of both steels (Fig. 1), it can be seen that in the hot-rolled bar (lower yield strength) the plastic zone after fatigue

pre-cracking is bigger, and the compressive residual stresses in the vicinity of the crack tip are extended along a broader region. This explains the result that the steel of highest yield strength (cold-drawn wire) is the most susceptible to hydrogen embrittlement.

The next step would be at least a first approach to the real residual stress distribution next to the crack tip. There are three kinds of difficulty in solving this problem. Firstly, from the theoretical point of view, it is impossible to know the exact stress distribution in the vicinity of the crack tip after fatigue pre-cracking (and therefore prior to the fracture test), because the stress singularity is relaxed by the plastification. In addition, the numerical approach to the problem (finite element method) is really complex due to the stress concentration and to the loading/unloading process. Finally, the residual stress distribution after fatigue pre-cracking is only representative at the beginning of the fracture test, since it changes during it. From these considerations it seems that the formulation of a simple model is sufficient indication of the residual stress distribution beside the crack tip.

In this paper, Rice's model [32] is used. It is applicable to an elastic ideally plastic material under cyclic loading, and predicts the residual stress distribution in front of the crack tip at the end of the final fatigue pre-cracking step, and therefore prior to the hydrogen embrittlement test. During this test the residual stresses in front of the crack tip are redistributed as the external load increases, and the compressions become tension.

Figure 9 shows the stress distribution proposed by Rice for the minimum ($K = K_{min}$) and maximum ($K = K_{max}$) fatigue loads. In both cases the maximum and minimum stresses are equal to the yield of the material $\sigma_Y$ (with positive and negative sign, respectively). The distribution

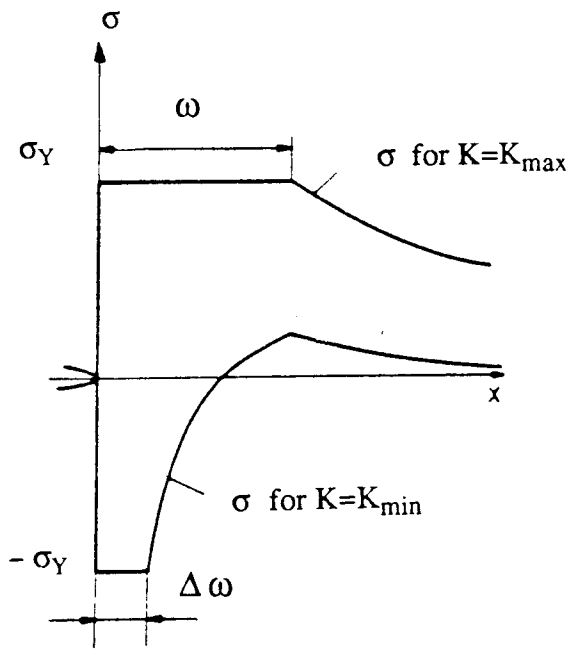


Fig. 9 Residual stress distribution in front of the crack tip, according to Rice's model (elastic ideally plastic material) [32].

corresponding to $K = K_{min}$ represents the stress state after fatigue pre-cracking (prior to the fracture test). As depicted in this plot, residual stresses ahead of the crack tip are compressions. The values of $\omega$ and $\Delta\omega$ are

$$\omega = \frac{\pi}{8}\left(\frac{K_{max}}{\sigma_Y}\right)^2 \tag{7}$$

$$\Delta\omega = \frac{\pi}{32}\left(\frac{\Delta K}{\sigma_Y}\right)^2 \tag{8}$$

where $\sigma_Y$ is the yield strength of the material, $K_{max}$ the maximum stress intensity factor during fatigue pre-cracking (last step of loading, just prior to the fracture test), and $\Delta K$ the stress intensity range in that step ($\Delta K = K_{max} - K_{min}$). In all cases $K_{min} \simeq 0$, and therefore $\Delta K \simeq K_{max}$. Designating $\lambda$ as the dimensionless ratio of the maximum stress intensity factor during fatigue pre-cracking to the fracture toughness, i.e.

$$\lambda = \frac{K_{max}}{K_{IC}} \tag{9}$$

we have

$$\omega = \frac{\pi}{8}\left(\frac{K_{IC}}{\sigma_Y}\right)^2 \lambda^2 \tag{10}$$

$$\Delta\omega = \frac{\pi}{32}\left(\frac{K_{IC}}{\sigma_Y}\right)^2 \lambda^2 \tag{11}$$

in which the ratio $K_{IC}/\sigma_Y$ is a characteristic of the material.

Rice's model does not take into account the strain-hardening of the material, and therefore the compressive residual stress at the boundary (crack tip) is always equal to the yield strength of the material. Despite this objection, it has been successfully used to study the fatigue growth of short cracks [33]. Moreover, the disregard of the strain-hardening of the material in this research is not a fundamental problem, since both steels have similar strain-hardening exponents.

On the other hand, the model is able to predict the depth of the maximum hydrostatic stress point, whose importance is determinant in hydrogen diffusion, as was demonstrated in previous research [34–36]. This point is always at a distance $\omega$ from the crack tip (Fig. 9).

Applying equation 10 and taking into account that the ratio $K_{IC}/\sigma_Y$ is 0.073 $m^{1/2}$ for the hot-rolled bar and 0.056 $m^{1/2}$ for the cold-drawn wire (see Table 2), the depth of the maximum hydrostatic stress point is as follows:

Hot-rolled bar: $\omega = 2.099\lambda^2$ (mm)
Cold-drawn wire: $\omega = 1.232\lambda^2$ (mm)

where $\lambda$ is the dimensionless ratio of $K_{max}$ to $K_{IC}$ (0.28, 0.45, 0.60 and 0.80). The value of $\omega$ is clearly higher for the hot-rolled bar. This length represents the distance which hydrogen has to cover to reach the critical point. The hydrogen concentration at such a point is higher for the cold-drawn wire, since it is nearer the crack tip. As a consequence, the fracture load in a hydrogen

environment, expressed as a percentage of the fracture load in air, is lower for the cold-drawn steel than for the hot-rolled one, as depicted in Figs 7 and 8.

These considerations explain why the cold-drawing process improves the mechanical properties of the steel while at the same time increasing its susceptibility to hydrogen embrittlement, a problem from this particular point of view.

Finally, a reflection on the effects of overloads on the life of prestressing steel wires in hydrogen environments. From the hydrogen embrittlement point of view, the application of overloads to the crack wires (obviously without exceeding the failure load) enlarges their life in the aggressive environment, because they produce a plastic zone in the vicinity of crack tips, thus generating compressive residual stresses which delay hydrogen entry. As is well known, this prestressing effect at the crack tip is also beneficial against fatigue crack propagation.

## 5. CONCLUSIONS

1. The higher-strength steel is more susceptible to hydrogen embrittlement than the lower-strength one. The cold-drawing process, from this point of view, is damaging, in spite of the improvement it imparts to the mechanical properties of the steel and to its behaviour in the EAC anodic regime.

2. The different susceptibility to hydrogen embrittlement as a function of the yield strength is explained on the basis of a non-conventional hydrogen diffusion model, which includes not only the hydrogen concentration, but also the hydrostatic stress distribution in the sample.

3. Rice's model of residual stress distribution in the vicinity of the crack tip after fatigue pre-cracking gives the depth of the point at which the hydrostatic stress reaches a maximum value (very important in hydrogen diffusion), and therefore explains the higher susceptibility of the cold-drawn wire to hydrogen embrittlement.

4. Compressive residual stresses generated in the vicinity of the crack tip during fatigue pre-cracking are relevant to the determination of the amount of hydrogen which fluxes into the sample, since those stresses delay the hydrogen diffusion.

5. The application of overloads to the cracked wire in a hydrogen environment is beneficial against hydrogen embrittlement and, as is well known, against fatigue crack growth.

## ACKNOWLEDGEMENTS

The authors would like to express their thanks to Professor Elices, head of the Material Science Department of the Polytechnical University of Madrid, for his encouragement and assistance.

## REFERENCES

1. Elices, M., 'Fracture of steels for reinforcing and prestressing concrete', in 'Fracture Mechanics of Concrete: Structural Application and Numerical Calculation' edited by G. C. Sih and A. DiTommaso (Martinus Nijhoff, Dordrecht, 1985) pp. 226–271.
2. McGuinn, K. F. and Elices, M., 'Stress corrosion resistance of transverse pre-cracked prestressing tendon in tension', *Br. Corros. J.* **16** (1981) 187–195.
3. Parkins, R. N., Elices, M., Sánchez-Gálvez, V. and Caballero, L., 'Environment sensitive cracking of pre-stressing steels', *Corros. Sci.* **22** (1982) 379–405.
4. FIP-78 (Stress Corrosion Test): 'Stress Corrosion Cracking Resistance for Prestressing Tendons', Technical Report No. 5.7 (International Prestressing Federation, Wrexham Springs, Slough, UK, 1981).
5. Elices, M., Sánchez-Gálvez, V. and Entrena, A., 'Stress corrosion testing of cold drawn steel wires in $NH_4SCN$ solution. $K_{ISCC}$ measurement', in Proceedings of 3rd International Prestressing Federation Symposium, Madrid, 1981.
6. Parkins, R. N., Elices, M. and Sánchez-Gálvez, V., 'Some comments on the standardization of tests methods for pre-stressing steel', *ibid.*
7. Elices, M., Maeder, G. and Sánchez-Gálvez, V., 'Effect of surface residual stress on hydrogen embrittlement of prestressing steels', *Br. Corros. J.* **18** (1983) 80–81.
8. Toribio, J. and Elices, M., 'Influence of residual stresses on hydrogen embrittlement susceptibility of prestressing steels', *Int. J. Solids Struct.* **28** (1991) 791–803.
9. Astiz, M. A., 'Estudio de la estabilidad de una fisura superficial en un alambre de acero de alta resistencia', PhD thesis, Polytechnical University of Madrid (1976).
10. Athanassiadis, A., Boissenot, J. M., Brevet, P., Francois, D. and Raharinaivo, A., 'Linear elastic fracture mechanics computations of cracked cylindrical tensioned bodies', *Int. J. Fract.* **17** (1981) 553–566.
11. Astiz, M. A., 'An incompatible singular elastic element for two- and three-dimensional crack problems', *ibid.* **31** (1986) 105–124.
12. Parkins, R. N., 'Development of strain-rate testing and its implications', in 'Stress Corrosion Cracking – The Slow Strain Rate Technique', STP 665, edited by G. M. Ugianski and J. H. Payer (ASTM, Philadelphia, Pennsylvania, 1979) pp. 5–25.
13. Scully, J. C., 'Propagation of stress corrosion cracks under constant strain-rate conditions', *ibid.* pp. 237–253.
14. Puiggali, M., Desjardins, D. and Ajana, L., 'A critical study of stress corrosion cracking testing methods for stainless steels in hot chloride media', *Corros. Sci.* **27** (1987) 585–594.
15. Lancha, A. M., 'Influencia del trefilado en la corrosión bajo tensión de aceros eutectoides', PhD thesis, Complutense University of Madrid (1987).
16. Brown, B. F., Fujii, C. T. and Dahlberg, E. P., 'Methods for studying the solution chemistry within stress corrosion cracks', *J. Electrochem. Soc.* **116** (1969) 218–219.
17. Barth, C. F., Steingerwald, E. A. and Troiano, A. R., 'Hydrogen permeability and delayed failure of polarized martensitic steels', *Corrosion–NACE* **25** (1969) 353–358.
18. Brown, B. F., 'Concept of the occluded corrosion cell', *ibid.* **26** (1970) 249–250.
19. Smith, J. A., Peterson, M. H. and Brown, B. F., 'Electrochemical conditions at the tip of an advancing stress corrosion crack in AISI 4340 steel', *ibid.* **26** (1970) 539–542.
20. Turnbull, A., 'The solution composition and electrode

potential in pits, crevices and cracks', *Corros. Sci.* **23** (1983) 833–870.
21. Etienne, C. F. and Wijngaard, B. H., 'Comparison of stress corrosion testing of prestressing steel under constant load and constant strain rate', in Proceedings of 3rd International Prestressing Federation Symposium, Madrid, 1981.
22. Tanaka, Y., Yamaoka, Y. and Karauchi, M., 'Effects of tensile strength on the stress corrosion behavior of steel wires in $NH_4SCN$ and $NH_4NO_3$ aqueous solutions', *ibid.*
23. Toribio, J. and Elices, M., 'Role of diffusion in the hydrogen transport in metals', in 'Fracture Behaviour and Design of Materials and Structures (ECF8)', edited by D. Firrao (Engineering Materials Advisory Service, West Midlands, UK, 1990) pp. 451–460.
24. Beck, W., Bockris, J. O., McBreen, J. and Nanis, L., 'Hydrogen permeation in metals as a function of stress, temperature and dissolved hydrogen concentration', *Proc. Roy. Soc.* **290** (1966) 220–235.
25. Bockris, J. O'M and Subramanyan, P. K., 'Hydrogen embrittlement and hydrogen traps', *J. Electrochem. Soc.* **118** (1971) 1114–1119.
26. Iino, M., 'Trapping of hydrogen by sulfur-associated defects in steel', *Metall. Trans.* **16A** (1985) 401–409.
27. Choo, W. Y. and Lee, J. Y., 'Effect of cold working on the hydrogen trapping phenomena in pure iron', *ibid.* **14A** (1983) 1299–1305.
28. Pound, B. G., 'The application of a diffusion/trapping model for hydrogen ingress in high-strength alloys', *Corrosion* **45** (1989) 18–25.
29. Van Leeuwen, H. P., 'The kinetics of hydrogen embrittlement: a quantitative diffusion model', *Engng Fract. Mech.* **6** (1974) 141–161.
30. Astiz, M. A., 'Hydrogen diffusion analysis in metals', in 'Computational Methods for Non-linear Problems', edited by C. Taylor, D. R. J. Owen and E. Hinton (Pineridge, Swansea, 1987) pp. 271–299.
31. Bockris, J. O'M. and Subramanyan, P. K., 'A thermodynamic analysis of hydrogen in metals in the presence of an applied stress field', *Acta Metall.* **19** (1971) 1205–1208.
32. Rice, J. R., 'Mechanics of crack tip deformation and extension by fatigue', STP 415, (ASTM, Philadelphia, Pennsylvania, 1967) pp. 247–309.
33. Pippan, R., 'The growth of short cracks under cyclic compression', *Fatigue Fract. Engng. Mater. Struct.* **9** (1987) 319–328.
34. Toribio, J. and Elices, M., 'Slow strain rate technique applied to round-notched wires', in Proceedings of Corrosion/88 (Corrosion Research Symposium), St. Louis, March 1988 (National Association of Corrosion Engineers) pp. 88–92.
35. Toribio, J. and Elices, M., 'Effect of local strain in stress corrosion testing', in 'Failure Analysis. Theory and Practice (ECF7)', edited by E. Czoboly (Engineering Materials Advisory Service, West Midlands, UK, 1988) pp. 1011–1013.
36. Toribio, J., Lancha, A. M. and Elices, M., 'Macroscopic variables governing the microscopic fracture of pearlitic steels', *Mater. Sci. Engng* **A145** (1991) 167–177.

## RESUME

**Influence du tréfilage sur la susceptibilité à la fragilisation à l'hydrogène de l'acier précontraint**

*On utilise couramment deux types d'aciers dans le béton armé: les aciers tréfilés (C–Mn) ou trempés (Si–Cr). Bien que leur limite élastique soit assez élevée pour garantir une durée de service normale dans la zone d'élasticité, leur résilience est moindre que celle des aciers ductiles de limite élastique inférieure, et ils sont, par conséquent, plus sujets à des défauts tels que fissures ou encoches. De plus, ces aciers peuvent se fissurer sous l'influence d'une ambiance corrosive. On compare ici le comportement, dans des conditions agressives, d'un acier de précontrainte C–Mn sous forme de barre ou de fil, de limites élastiques différentes, afin d'étudier l'influence de ce paramètre du matériau sur la fissuration favorisée par l'hydrogène en milieux aqueux et, par suite, l'effet (bénéfique ou non) du procédé de tréfilage de ce point de vue particulier. Le programme expérimental consistait en une série d'essais de déformation à vitesse lente sur des éprouvettes pré-fissurées dans des conditions ambiantes variées. On a utilisé différentes charges de pré-fissuration en fatigue pour analyser l'influence de l'état de contrainte au voisinage de l'extrémité de la fissure sur le processus de fissuration favorisé par l'hydrogène. Les résultats confirment le fait bien connu, à savoir que le fil tréfilé (acier de haute résistance) est davantage sujet à la fragilisation par l'hydrogène que la barre laminée à chaud (résistance plus basse), ce qui montre que le tréfilage réduit la résistance d'un acier de précontrainte à la fissuration favorisée par l'hydrogène.*

*Dans la partie théorique, on propose un modèle de diffusion de l'hydrogène dans les métaux—qui tient compte des effets de la concentration en hydrogène et de la distribution des contraintes hydrostatiques—pour expliquer les résultats expérimentaux à partir de la courbe contrainte/déformation établie pour chaque matériau. On tient compte des contraintes en compression résiduelles qui se produisent au voisinage de l'extrémité de la fissure pendant le processus de pré-fissuration en fatigue, et qui sont modélisées selon les distributions de Rice pour un matériau élastique idéalement plastique. Le modèle permet d'expliquer les différentes susceptibilités à la fragilisation à l'hydrogène des deux formes d'acier de précontrainte à haute résistance (barre et fil): après la pré-fissuration en fatigue, la barre laminée à chaud présente une zone plastique plus large que le fil tréfilé, et l'hydrogène doit couvrir une plus longue distance avant d'atteindre le point critique, ce qui explique pourquoi la barre laminée est moins susceptible à la fragilisation à l'hydrogène.*